Case Study for Seismic Assessment of an Existing Asymmetric non-prismatic Unique Reinforced Concrete-encased Steel Plate Column in Wellington

A. Moshref, E. Bigsby
Miyamoto International NZ, New Zealand

M. Khanmohammadi, M. Katrangi
School of Civil Engineering, College of Engineering, University of Tehran, Iran

This case study presents a tailored approach to assessing a high-rise building in the Wellington CBD constructed primarily from reinforced concrete-encased steel frames. This construction is rare in New Zealand, and it is fascinating the way the building has been designed. Due to the singular nature of the building, traditional seismic assessment guidance is difficult to employ and a unique approach to the analysis is required.

The structure is a 16-storey tower building on a 6-storey podium designed and constructed in the mid-1960s. The main structure at the perimeter consists of steel truss beams and flanged steel columns all encased in concrete. The podium perimeter structure consists of concrete-encased steel braced frames and shear walls.

This paper presents a finite element modelling (F.E.M) assessment for the main corner columns at the 7th story which consists of an asymmetric non-prismatic steel braced frame encased in reinforced concrete. This column type has not been investigated so far, based on the authors' survey. In absent of any guideline design or assessment for such elements, using F.E.M can provide an acceptable insight to study the seismic performance and responses. This paper presents the results of F.E.M using DIANA software in order to estimate both flexural and shear responses as well as failure mode. The results show that the behaviour of these columns are categorized as flexure-shear for critical section at base of column. The results are used in seismic assessment of building as whole.

1 INTRODUCTION

Concrete-encased steel columns are widely used in high-rise building all over the world due to the high performance level under seismic and gravity loads. There are many types of composite columns, classified according to the position of the steel plate, longitudinal profiles and the column shape as shown in Figure 1. Many experimental tests have been performed to obtain the lateral response of concrete-encased steel columns

by many researchers (Suzuki et al. 1984) (Viest et al. 1997) (Chen 2007) (Chen et al 2014). The experimental tests results revealed that encasing the steel section in concrete provides high shear capacity, stiffness and ductility and large energy absorption, while the surrounding concrete protects the steel elements from fire damage and delays the buckling failure. There are many factors that control the seismic response of composite column such as the axial load ratio, aspect ratio, steel ratio and reinforcement ratio. To deeply understand the modes of failure and the key parameters that influence the composite column behaviour, a comprehensive parametric study using FE analyses was conducted by Ellobody and Young (Ellobody and Young 2011). Additionally, a comparative numerical study on the encased steel composite columns and steel columns was performed by Lacki et al. (Lacki 2018). The previous studies focused on the performance of the rectangular or circular concrete-encased columns with steel profiles distributed in symmetric manner across the column section. In some old high-rise building, it was noticed that a prismatic concrete-encased steel column was used in some cases, such as the Morrison Kent House building designed and constructed in the mid-1960s. In such cases, the composite column may behave with a different response in comparison with the conventional concrete-encased steel column. In this study, a proved-reliable finite element model for assessment the seismic response of prismatic concrete-encased steel columns is provided using DIANA software (DIANA FEA 2016). Non-linear static pushover analyses were performed to obtain the column behaviour under lateral and gravity loads. To this end, the gravity load level was varied to cover the axial load variations under earthquake load case.

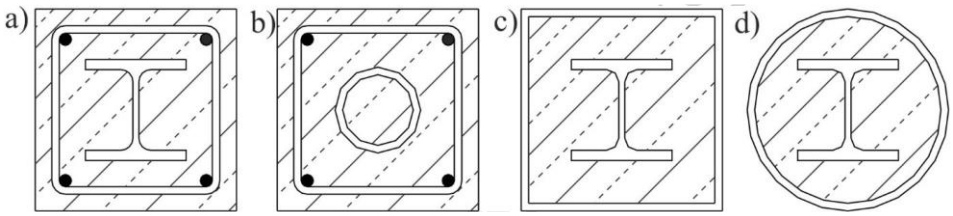

Figure 1: Some type of composite columns: a) steel reinforced concrete (SRC), b) Concrete Filled Steel Tube (CFST), c) square tubed SRC (STSRC), d) circular tubed SRC (CTSRC).

2 CASE STUDY OF CONCRETE -ENCASED STEEL- COLUMNS

The Morrison Kent House building is used in this paper as a case study. The structure is a 23-storey building comprising a sixteen-storey tower supported by a six-storey podium structure, which was designed and constructed circa 1964-65. The total height of the building is 78m above foundation level and the height of the main tower is 51m (above podium). The main structure at the perimeter consists of steel truss beams and flanged steel columns all encased in concrete. The podium perimeter structure consists of concrete-encased steel braced frames and shear walls. The lateral load resisting system of the building consists of reinforced concrete-encased structural steel latticed frames around the perimeter of the tower and reinforced concrete-encased braced steel frames along podium boundary walls. The perimeter reinforced concrete-encased structural steel frames comprise of a plate steel truss system for the beams and beam-column joints, with columns constructed from a flanged steel section made up from prefabricated web and flange plates. Figure 2 shows the truss arrangement for the perimeter frame structure. In Figure 2, the corner column of the composite truss frame, that is a non-prismatic element, is selected as a study case due to its geometry complexity and the asymmetric distribution of the flanged steel sections. The configuration of the selected composite column is presented in Figure 3.

3 FINITE ELEMENTS MODELLING

3.1 Modelling Approach

Three-dimensional (3D) twenty-node isoparametric solid brick elements are used to simulate the concrete, flanged steel sections, battens and the joint steel plates, which is based on quadratic interpolation and Gauss integration; while reinforcing bars are modelled by the embedded reinforcement technique. In material modelling, the concrete models are based on nonlinear fracture mechanics to account for cracking, and plasticity models are used for the concrete in compression and steel reinforcement.

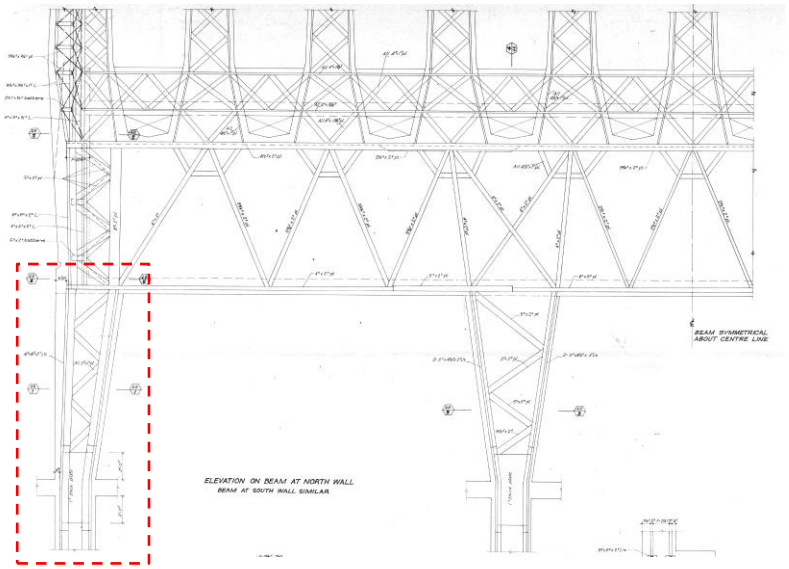

Figure 2: The truss arrangement for the perimeter frame structure.

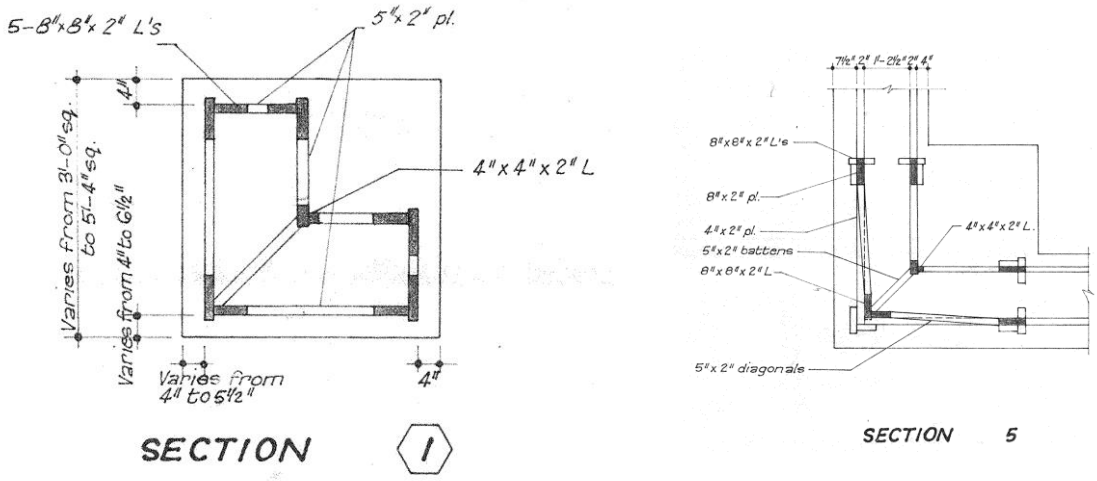

Figure 3: Concrete-Encased Steel- Column configurations.

By considering the complicated geometry of the model, firstly the concrete and steel elements have been separately generated. In the second stage and for processing the overlapping in model geometry, the steel profiles volumes were subtracted from the surrounding concrete elements and then the interfaces between the steel and concrete were defined using a nonlinear slip material. The total strain rotating crack model is used to simulate the cracking characteristics of concrete, in the sense that when the principal tensile stress exceeds the specified limiting value, cracks will occur in the perpendicular direction. The rotating crack model was selected here in consideration of its simplicity and reasonable accuracy. Hence in this analysis, the shear retention factor was assumed to be one, which means that shear modulus is constant before and after cracking. Figures 4 and 5 show the geometry and the mesh (100x100x100 mm) of the model.

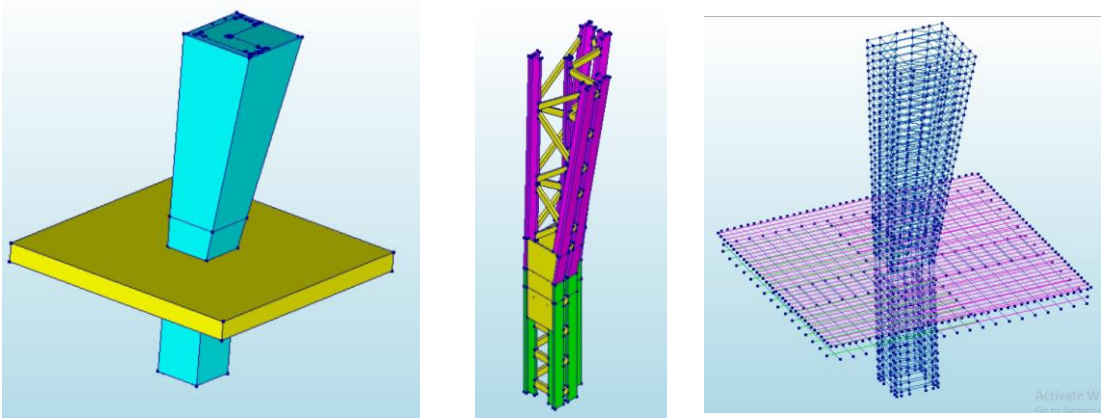

(a) Concrete elements *(b) Steel elements* *(c) reinforcement*

Figure 4. Finite element modelling.

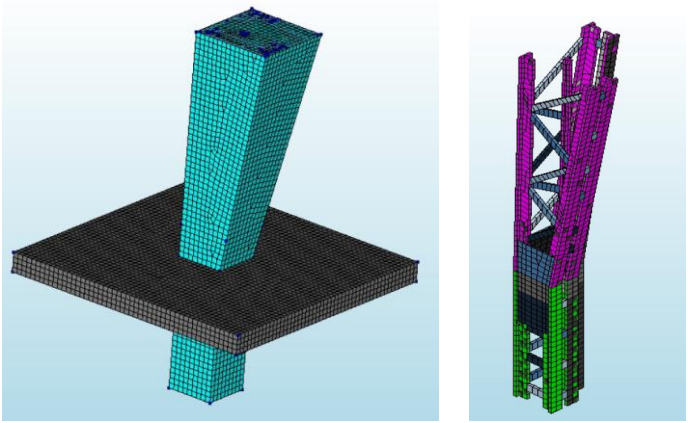

Figure 5. Mesh size for Model.

3.2 Concrete and Steel Stress-Strain Relationships

The parabolic compressive stress-strain relationship was used for the unconfined concrete in the analysis as shown in Figure 6 (a). The parabolic compressive stress-strain relationship of concrete is defined by:

$$\sigma = \begin{cases} -f_c \dfrac{\varepsilon_j}{3\varepsilon_{c/3}} & \varepsilon_{c/3} < \varepsilon_j \le 0 \\ -f_c \dfrac{1}{3}\left(1 + 4\left(\dfrac{\varepsilon_j - \varepsilon_{c/3}}{\varepsilon_c - \varepsilon_{c/3}}\right) - 2\left(\dfrac{\varepsilon_j - \varepsilon_{c/3}}{\varepsilon_c - \varepsilon_{c/3}}\right)^2\right) & \varepsilon < \varepsilon_j \le \varepsilon_{c/3} \\ -f_c\left(1 - \left(\dfrac{\varepsilon_j - \varepsilon_c}{\varepsilon_u - \varepsilon_c}\right)^2\right) & \varepsilon_u < \varepsilon_j \le \varepsilon_c \end{cases} \quad (1)$$

$$\varepsilon_{c/3} = -\frac{f_c}{2E}$$
$$\varepsilon_c = -\frac{5f_c}{3E} = 5\varepsilon_{c/3} \quad (2)$$
$$\varepsilon_u = -\frac{3G_c}{2hf}$$

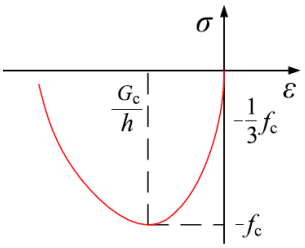

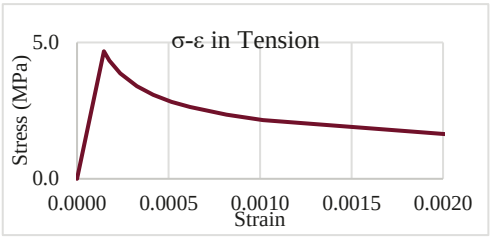

(a) Concrete in compression *(b) Concrete in tension*

Figure 6. Stress-strain relationship model of concrete.

Where, $G_c = 250.G_f$ is the total compressive fracture energy of concrete and, G_f is the fracture energy in tension was estimated using CEB-FIP Model (CEB-FIP Code 1990).

Concrete in tension (Figure 6 (b)) was modelled using (Belarbi and Hsu 1996) model that is defined as follows [2]:

$$\sigma r = EC \times \varepsilon r \qquad \varepsilon r \leq \varepsilon cr \quad (3)$$

$$\sigma r = fcr \times \left(\frac{\varepsilon cr}{\varepsilon r}\right)^{0.4} \qquad \varepsilon r > \varepsilon cr \quad (4)$$

Where, Ec is the modulus of concrete; fcr is the tensile strength of the concrete, and εcr is the average tensile strain at which the concrete begins cracking, given as $\varepsilon cr = fcr/Ec$. The ultimate tensile strain εtu is calculated based on the following equation.

$$\varepsilon tu = \varepsilon t - 0.0004 fcr \quad (5)$$

The embedded reinforcement technique was chosen for the modelling of reinforcement bars which allowed for less computation and easier modelling. The tri-linear stress-strain model, as shown in Figure 7, was used for simulating the reinforcing bars and the shaped steel.

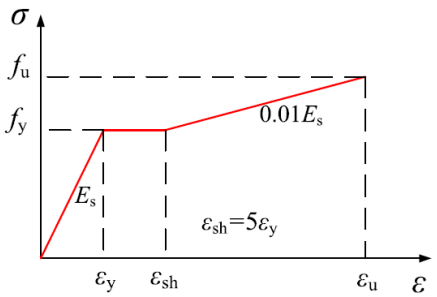

Figure 7. Stress-strain relationship of steel.

3.3 Bond Slip Between Steel Plates and Concrete

In this study the local bond–slip behaviour between the steel plate and concrete is assumed to have a bi-linear shape (Majdi et al. 2014). As shown in Figure 8, the local bond–slip relationship comprises an ascending branch and a descending (softening) branch. This model is described by the following equations using SI units:

$$\tau_f = -0.054 f_c' + 0.7\sqrt{f_c'} - 1.193 \quad (6)$$

$$\delta_f = 9.373 \sqrt{f_c'} + 8.123 \quad (7)$$

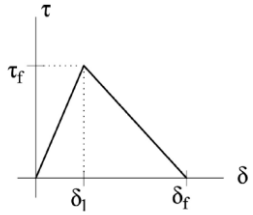

Figure 8. Bond slip model between steel plate and concrete panel[3].

3.4 Boundary Condition and Load Cases

In this study, three boundary conditions presented in Figure 9 are considered. For obtaining the bottom section behaviour of the top column, the slab and the bottom column are fixed in the x, y and z directions and the lateral load is applied at the top of the column. In the second boundary conditions, the top section is fixed in the x, y and z directions to obtain the behaviour of the top column at the top section. Finally, for analysing the bottom column the slab and the top column are fixed in the x, y and z directions. Non-linear Static Pushover analysis is performed to obtain the column behaviour under lateral and gravity loads. Three cases for gravity loads are considered to cover the axial load variations during the earthquake. The values of 0, 6500 and 10000kN are considered in analysing the critical section of each section of the composite column.

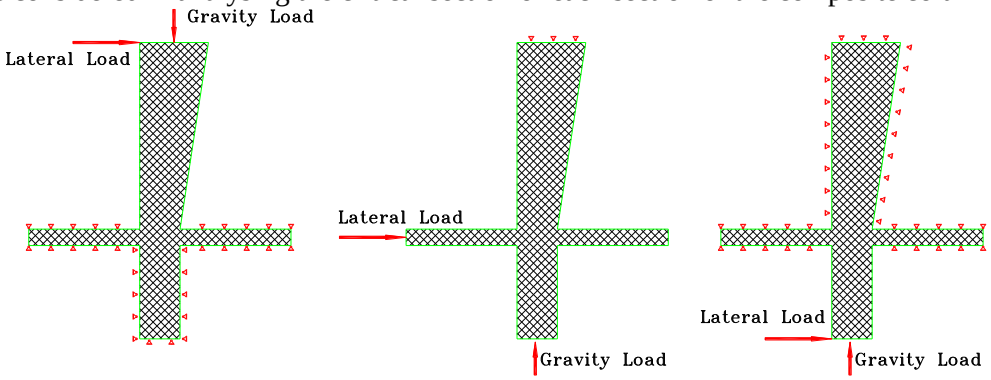

(a) Boundary Condition 1 *(b) Boundary Condition 2* *(c) Boundary Condition 3*

Figure 9. FE-Boundary Conditions

4 ANALYSIS RESULTS

For assessment of the nonlinear seismic behaviour of the composite column, pushover analyses were carried out after applying the gravity loads for the three mentioned cases. Due to the asymmetric geometric of the model, the lateral displacement was applied in the positive and negative directions of the X axis to obtain the positive and negative capacities of the section. The pushover curves (lateral load versus lateral drift) are shown in Figure 10. Figures 11-13 show the steel shape, concrete and reinforcement plastic strains, respectively. On the other hand, for obtaining the shear capacity of the top column the pushover analysis was performed by applying the lateral displacement 1m from the slab level so that the aspect ratio is one. Figure 10 bottom right shows the shear capacity versus lateral drift of the top column at the bottom section.

The results showed that the top column response was not symmetric in the positive and negative directions, while no noticeable difference was observed for the bottom column. Increasing the axial load force led to an increase in the column capacity, but at the same time the strength degradation occurred at a smaller drift ratio. The bottom column performed better than the top column and the strength degradations was not sharp as in the top column. Under the lateral loads, the concrete in the top column failed in compression in a non-ductile manner, especially at the corner that had no steel profiles. Following concrete compression failure, the steel profiles and the longitudinal rebars buckled at a drift between 1.0-1.5% corresponding to the axial load level. The same results were obtained for the top section of the top column but for drift between 1.5-2.0%. The shear capacity of the column is between 5700-7300kN corresponding to axial load level. This indicates that the failure mode of the column is flexure-shear and closer to shear failure. It is noted that to determine the shear capacity the same model of condition 1 of Figure 9 is used but the location of lateral load is placed at the height of 0.8m from the base to provide a shear span to depth ratio of less than 1.0. Figure 10 (bot. right) illustrate the derived responses regarding different axial loads.

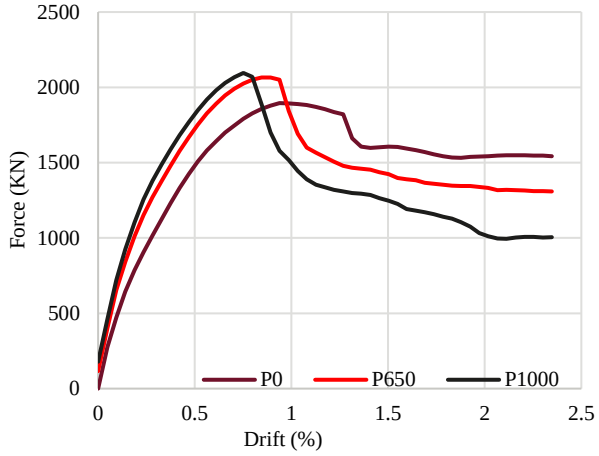

a) Top Column, Bottom Section, Positive

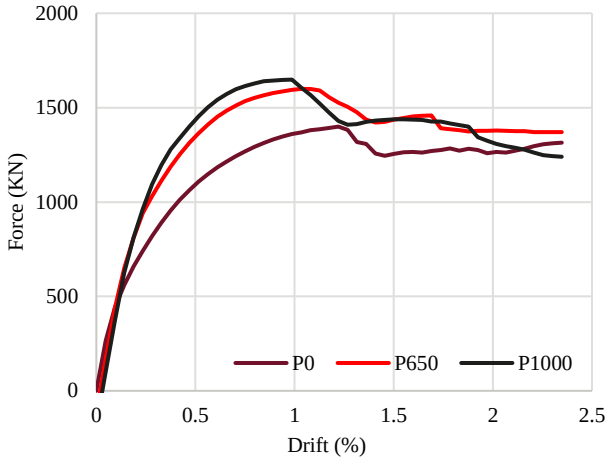

b) Top Column, Bottom Section, Negative

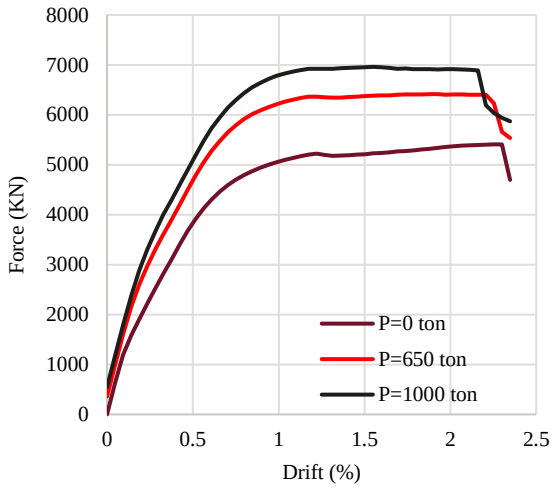

c) Top Column, Top Section, Positive

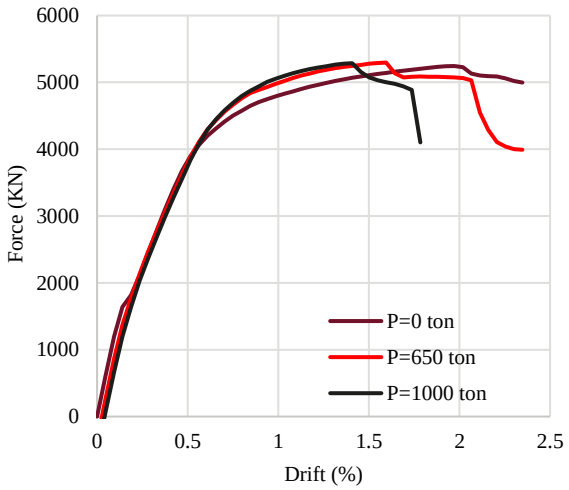

d) Top Column, Top Section, Negative

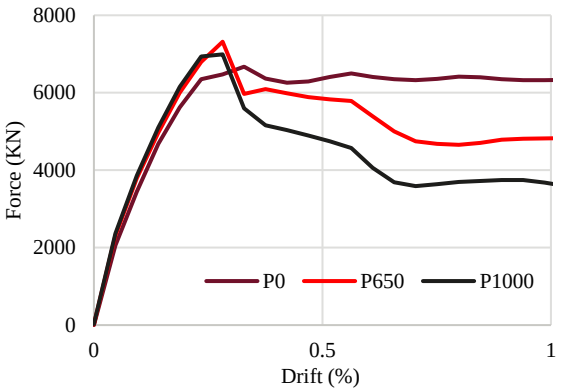

d) Shear capacity of Top Column, Bottom Section, Positive

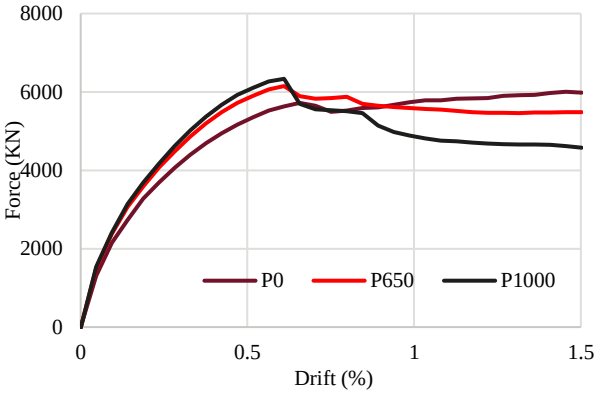

e) Shear Capacity of Top Column, Bottom Section, Negative

Figure 10. Column lateral force versus lateral drift.

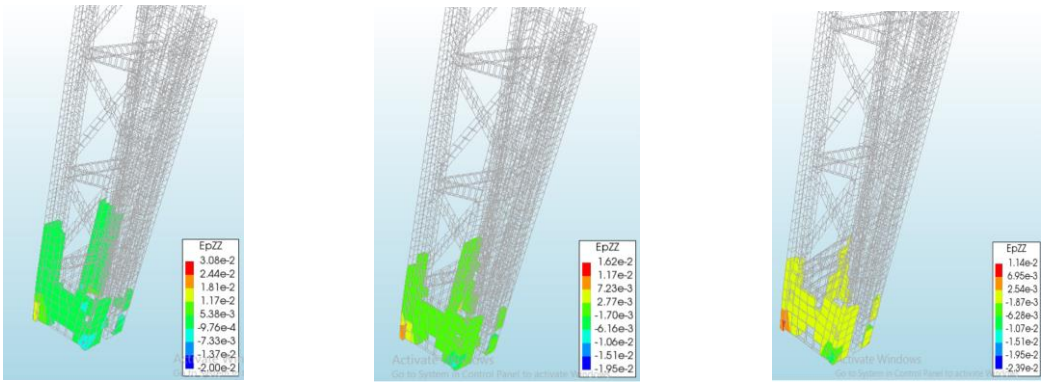

(a) Case1 (N=0kN) *(b) Case2 (N=6500kN)* *(c) Case3 (N=10000kN)*

Figure 11. Strains of steel elements (positive)

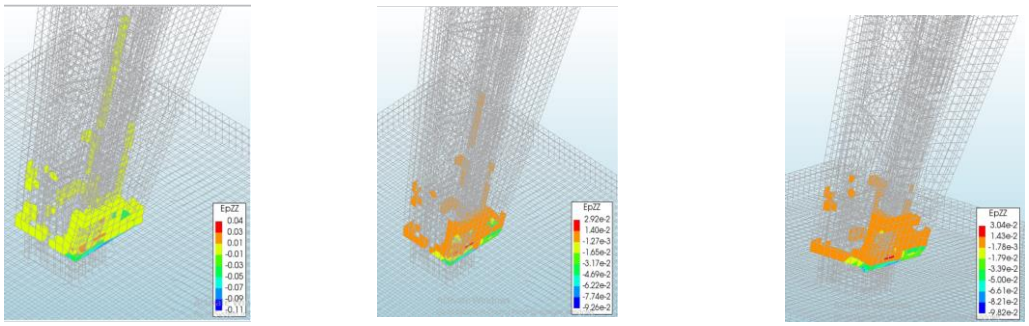

(a) Case1 (N=0kN) *(b) Case2 (N=6500kN)* *(c) Case3 (N=10000kN)*

Figure 12. Strains of concrete (positive)

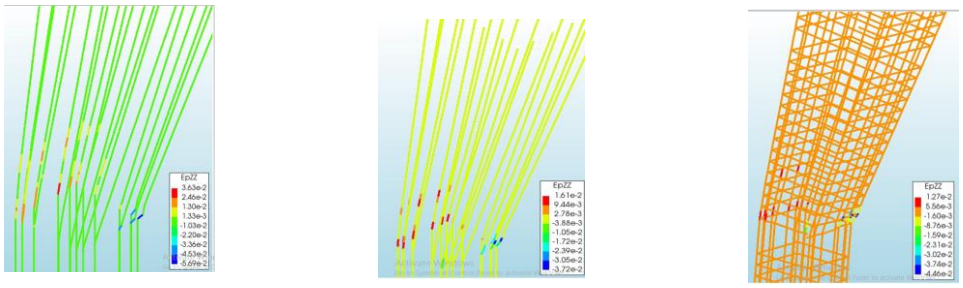

(a) Case1 (N=0kN) *(b) 2 6500kN)* *(c) Case3 (N=10000kN)*

Figure 13. Strains of reinforcement (positive)

5 CONCLUSION

A unique concrete-encased steel composite column was analysed under lateral and gravity loads as a case study for assessment the seismic response of the non-conventional composite column. The steel profiles of the column are distributed in an asymmetric manner and the lateral confinement conditions do not satisfy confinement requirements. The gravity load and the boundary conditions have been changed to cover all critical cases the during the earthquake. The following conclusion can be drawn:

1- For the bottom section of the top column. When the column is subjected to bending action (Lateral load applied at the top of the column), the concrete fails in compression and the longitudinal rebars buckle in low strains at a drift between 1.0-1.5% corresponding to the axial load level. The lateral response is not symmetric – when the column edge without a steel profile is subjected to compression, the concrete fails in a non-ductile manner and controls the column behaviour.

2- The shear capacity of the top column is between 5700-7300kN corresponding to axial load level. This indicates that the failure mode of the column is flexure-shear and improving shear capacity is suggested if necessary.

REFERENCES

Belarbi, A., Zhang, L. X., & Hsu, T. T. (1996). Constitutive laws of reinforced concrete membrane elements. In Sociedad Mexicana de ingenieria sismica in world conference on earthquake engineering (pp. 1-8).

Chen, C. H. (2007). Experimental study and numerical analysis on steel reinforced concrete compression-bending members. Technical Rep., China Academy of Building Research, Beijing (in Chinese).

Chen, C., Wang, C., & Sun, H. (2014). Experimental study on seismic behaviour of full encased steel-concrete composite columns. Journal of Structural Engineering, 140(6), 04014024.

Comité Euro-International du Béton. CEB-FIP model code 1990: Design code. Thomas Telford Publishing; 1993.

DIANA FEA 10.1. Delft (The Netherlands): TNO DIANA BV; 2016.

Ellobody, E., & Young, B. (2011). Numerical simulation of concrete-encased steel composite columns. Journal of Constructional Steel Research, 67(2), 211-222.

Lacki, P., Derlatka, A., and Kasza, P. (2018). Comparison of steel-concrete composite column and steel column. Composite Structures, 202, 82-88.

Majdi, Y., Hsu, C. T. T., and Punurai, S. (2014). Local bond–slip behavior between cold-formed metal and concrete. Engineering structures, 69, 271-284.

Suzuki, T., Takiguchi, K., Ichinose, T., & Okamoto, T. (1984). Effects of hoop reinforcement in steel and reinforced concrete composite sections. Bulletin of the New Zealand Society for Earthquake Engineering, 17(3), 198-214.

Viest, I. M., Colaco, J. P., Furlong, R. W., Griffis, L. G., Leon, R. T., and Wyllie, L. A. (1997). Composite construction: design for buildings. McGraw-Hill, New York.